LANGMUIR

pubs.acs.org/Langmuir Article

Free-Rising Bubbles Bounce More Strongly from Mobile than from Immobile Water–Air Interfaces

Ivan U. Vakarelski,* Fan Yang, and Sigurdur T. Thoroddsen

Cite This: *Langmuir* 2020, 36, 5908–5918 Read Online

ACCESS | Metrics & More | Article Recommendations | Supporting Information

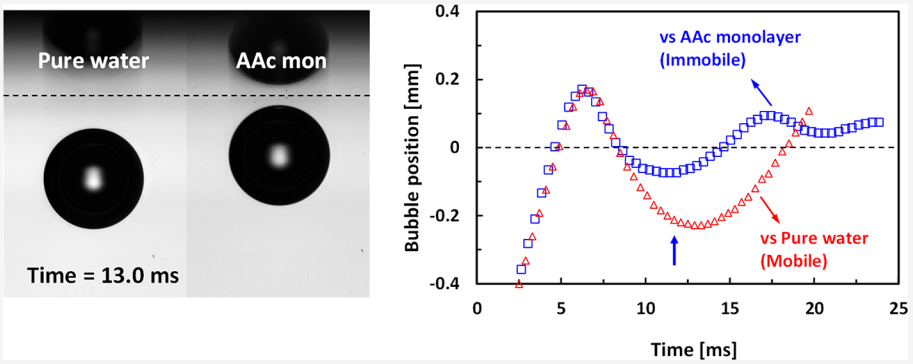

ABSTRACT: Recently it was reported that the interface mobility of bubbles and emulsion droplets can have a dramatic effect not only on the characteristic coalescence times but also on the way that bubbles and droplets bounce back after collision (Vakarelski, I. U.; Yang, F.; Tian, Y. S.; Li, E. Q.; Chan D. Y. C.; Thoroddsen, S. T. *Sci. Adv.* **2019**, *5*, eaaw4292). Experiments with free-rising bubbles in a pure perfluorocarbon liquid showed that collisions involving mobile interfaces result in a stronger series of rebounds before the eventual rapid coalescence. Here we examine this effect for the case of pure water. We compare the bounce of millimeter-sized free-rising bubbles from a pure water–air interface with the bounce from a water–air interface on which a Langmuir monolayer of arachidic acid molecules has been deposited. The Langmuir monolayer surface concentration is kept low enough not to affect the water surface tension but high enough to fully immobilize the interface due to Marangoni stress effects. Bubbles were found to bounce much stronger (up to a factor of 1.8 increase in the rebounding distance) from the clean water interface compared to the water interface with the Langmuir monolayer. These experiments confirm that mobile surfaces enhance bouncing and at the same time demonstrate that the pure water–air interfaces behave as mobile fluid interfaces in our system. A complementary finding in our study is that the ethanol–air interface behaves as a robust mobile liquid interface. The experimental findings are supported by numerical simulations of the bubble bouncing from both mobile and immobile fluid interfaces.

INTRODUCTION

The dynamic interaction between deformable bubbles and droplets are of continued research interest because of their involvement in numerous industrial applications, naturally occurring phenomena, and biological processes.[1−8] The outcome of the collision between two bubbles or droplets is primarily determined by the hydrodynamic interaction that acts from separation distances comparable to the size of bubbles and droplets down to the submicrometer thicknesses of the thin liquid film formed between the two colliding surfaces. The hydrodynamic interaction itself is a strong function of the mobility of the bubble or droplet liquid interface.[9−14] A clean bubble or droplet interface is expected to be tangentially mobile. In contrast, along a liquid–solid interface the liquid molecules are immobile and the fluid velocity is zero, or what is known as the no-slip boundary condition.

In practical situations the adsorption of surface active molecules at the gas–liquid or liquid–liquid interface can effectively immobilize the interface due to Marangoni stress related effect and make it behave as a solid interface.[12−15] For a gas–liquid interface, because of the large difference between the gas and liquid viscosities, the interface cannot sustain any significant tangential stress, which is referred to as fully mobile or a free-slip liquid interface. For a clean liquid - liquid interface the mobility is determined by the ratio of the liquids viscosities. A droplet with much lower viscosity than the

Received: March 10, 2020
Revised: May 7, 2020
Published: May 7, 2020

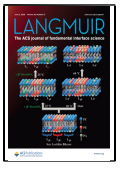

https://dx.doi.org/10.1021/acs.langmuir.0c00668
Langmuir 2020, 36, 5908–5918

surrounding liquid will behave as a stress-free interface gas bubble. On the other hand, a droplet with much higher viscosity than the surrounding liquid will behave like a no-slip interface solid particle.

For simplicity, from here on we will refer to a clean gas−liquid interface, which is tangentially mobile as mobile fluid interface and to a gas−liquid interface which is tangentially immobilized due to surface-active components' adsorption as immobile fluid interface. It is generally expected that two mobile-surface bubbles or droplets, which do not bounce back after collision, will coalesce much faster due to the lower hydrodynamic resistances during approach compared to immobile interface bubbles or droplets.[11,14]

The mobility of gas bubbles and liquid droplets in water, the most practically relevant liquid, is often problematic to determine due to the high affinity of surface-active contaminants or added surfactants to the water interface. An important consideration when discussing the mobility of the water−air interface is the hydrodynamic regime and related shear stress in the system. Small bubbles in the submillimeter size range freely rising in the Stokes flow regime are extremely sensitive to the presence of minute amounts of contaminates and will be immobilized at surfactant concentrations which are too low to be detected by the change in the water−air interfacial tension.[12−18] A recent work has also hypothesized that mobile surface charge adsorption at the water interface can also contribute to the immobilization of the water−air interface.[15] However, larger bubbles (of millimeter size) are shown to rise as a tangentially mobile interface if no added surfactant is present in the water.[19−22] Finally, for macroscopic bubbles and high shear rates as in foam shear experiments[23] or in the free-fall of centimeter-sized spheres with attached air cavities,[24,25] the bubble interface can be mobile even when a high concentration of low-modulus surfactants is present in the water.

To study the effect of the interface mobility on the bubbles and droplets coalescence dynamics, we have recently conducted experiments using extrapure perfluorocarbon liquids. The perfluorocarbon liquids have excellent resistivity to surface-active contaminants, which leaves the liquid−air interface inherently mobile. The first study[26] was conducted using the perfluorocarbon liquid, PP11 (perfluoroperhydrophenanthrene, $C_{14}F_{24}$, F2 Chemicals), that has a viscosity that is about 20 times higher than that of water. Using a higher-viscosity liquid allowed us to study rising bubbles colliding with the interface in the Stokes regime, in which case it is easy to confirm that both the bubble and the free interface behave as robust contaminant-resistant mobile fluid interfaces. In a companion study,[27] we used the perfluorocarbon liquid, PP1 (perfluoro-2-methylpentane, C_6F_{14}, F2 Chemicals), which has a viscosity close to that of water. In these earlier experiments, we compare the bounce of a free-rising air bubble or a water droplet from the mobile PP1−air interface with the bounce from a PP1−water interface immobilized by the addition of surfactant to the water phase. It was found that the bubble collision with the mobile PP1−air interface results in a significantly stronger series of rebounds before rapid coalescence compared to the bounces from the immobile PP1−water interface. The stronger rebounds from the mobile interface were explained with the reduced viscous dissipation compared to collisions involving immobile interfaces. The enhanced bounce from mobile interfaces was confirmed by numerical simulations of a free-rising bubble bouncing from an interface.[27]

In the present work, we aim to extend the investigation of the effect of the fluid interface mobility on the bubble collision dynamics by conducting experiments on free-rising bubbles bouncing off of the water−air interface. We also present some reference results for bubble bouncing from the ethanol−air interface. For the case of water, we take advantage of the fact that the water−air interface can be immobilized by the deposition of insoluble surfactants at the water interface (e.g., by the deposition of a Langmuir monolayer[28,29] at the water−air interface). The Langmuir monolayer surfactant concentration can be chosen to be low enough not to change the water surface tension significantly but high enough to immobilize the interface due to Marangoni stress effects.

EXPERIMENTAL SECTION AND NUMERICS

Materials and Experimental Setup. Water was purified in a Millipore apparatus with an internal specific electrical resistance of no less than 18.4 MΩ/cm. No additional water purification by distillation was needed to observe bubble rising velocities consistent with the tangentially mobile behavior, over the range of the bubble sizes used herein of 0.6 to 1.5 mm. Ethanol of >99.7% absolute grade used in the bubble rise experiments was purchased from VWR Chemicals and used without further purification. Arachidic acid (AAc, ≥99%), sodium dodecyl sulfate (SDS), and chloroform were from Sigma-Aldrich. All experiments were conducted at laboratory room temperature of about 21 °C.

The schematic of the experimental setup used to monitor the bubble free rise and collision with a liquid interface is shown in Figure 1a. In essence, this is the same experimental setup that we used in our recent studies[26,27] on bubble rise and coalesce in perfluorocarbon liquids. In the present study, the glass container was an optical glass cell purchased from Hellma Analytics, with a cross section of 5.0 × 4.0 cm and a height of 10.0 cm. A small hole was drilled through the bottom of the cell into which a glass microcapillary of 50 or 100 μm inner diameter was inserted. The capillary is connected by a plastic tube to a pressure regulator (Iwashita Instruments Ltd.) used to generate controlled pressure-driven air-flow pulses. Using combinations of different air pressure and pulse duration, we were able to release from the end of the capillary air bubbles with diameters in the range of 0.6 to 1.5 mm.

The bubbles' free rise and collision with the top surface were recorded using a high-speed camera (Photron-SA5) equipped with a long-distance microscope with a 5× magnification objective (Mitutoyo), giving a resolution of 4.0 μm/pixel. The high-speed videos were taken using a typical rate of 5000 frames per second (fps) at a shutter speed of up to 1/15 000 s to avoid image seaming for sharper contrast. The time trajectories of the bubble center-of-mass position were determined by image processing the videos using an in-house-developed MATLAB image processing code.

Before the experiments, the glass vessel was plasma cleaned and washed with a copious amount of deionized water. The experiments were conducted shortly after the clean vessel was filled with Millipore purified water. In all experiments, bubbles were released from at least 2.5 cm below the water−air surface to ensure that the bubbles reach terminal velocity before collision with the interface. For the range of bubble sizes studied, from 0.7 to 1.5 mm of undeformed bubble diameters, the bubbles assume an oblate ellipsoidal shape as schematized in Figure 1c. In this case, it is convenient to characterize the bubble using the equivalent diameter, $D \equiv (D_h^2 D_v)^{1/3}$, where D_h and D_v are the horizontal and vertical ellipsoid diameters. The position of the bubble center-of-mass progression with time, $H(t)$, is measured relative to the undeformed interface, with the $H = 0$ position corresponding to the undeformed bubble coming in contact with the undeformed interface (Figure 1c). For an undeformed spherical bubble approaching an undeformed flat interface, $H(t)$ also

https://dx.doi.org/10.1021/acs.langmuir.0c00668
Langmuir 2020, 36, 5908−5918

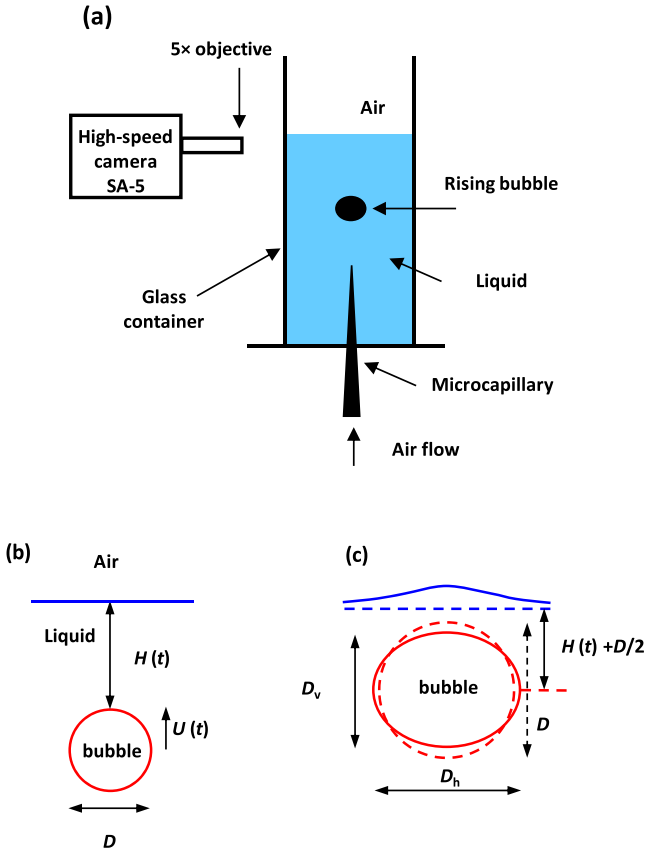

Figure 1. (a) Schematic of the experimental setup. (b) Schematic of a spherical bubble rising toward an undeformed liquid−air interface. (c) Schematic of an oblate ellipsoidal bubble of horizontal diameter D_h and vertical diameter D_v approaching a deformable interface. Blue dashed lines denote the position of the undeformed interface, and an undeformed bubble of diameter $D \equiv (D_h^2 D_v)^{1/3}$ is indicated by the red dashed line. The bubble center-of-mass position, relative to the horizontal reference position, is $H(t)$ as indicated, with $H(t) = 0$ corresponding to the top of an undeformed bubble reaching the undeformed interface.

equals the distance between the top of the bubble and the interface (Figure 1b).

Arachidic Acid Langmuir Monolayer Preparation and Characterization. The arachidic acid (AAc) Langmuir monolayer was formed on the water interface by using a standard procedure for monolayer deposition in a Langmuir−Blodgett trough apparatus. First we prepare a 0.1 wt % solution of AAc in chloroform. Then, using a micropipet, about 6 μL of the chloroform solution was deposited dropwise on top of the water interface in the liquid vessel. The surface area of the experimental vessel is about 20 cm^2. In less than a minute, the chloroform solution droplets fully evaporate from the interface. Measurement of the surface tension of water for a monolayer of the same surface concentration of AAc made with a Kruss tensiometer, using the Wilhelmy plate method, gave a value of 72.4 ± 0.1 mN/m, which, within experimental error, was the same as that for a clean water surface before the monolayer deposition. When the AAc surface concentration was doubled to 12 μL for the 0.1 wt % AAc in chloroform, the surface tension fell to 61.4 ± 0.1 mN/m. We estimated the AAc molecular area to be about 55 Å^2 when 6 μL of the chloroform solution was deposited and about 27.5 Å^2 for the 12 μL deposition. These areas are in agreement with the surface tension measurement, with 55 Å^2 corresponding to a "gas" state of the molecules on the interface and thus not affecting the surface tension, while the 27 Å^2 is in the range of the "liquid" state of the molecules in the interface, which is expected to decrease the surface tension.[29] Therefore, in all of our experiments we use the 6 μL droplet of the 0.1 wt % AAc chloroform solution to produce an immobile water interface.

Gerris Numerical Simulation (GNS). As in our recent work on bubbles bouncing from interfaces in perfluorocarbon liquid PP1,[27] we conducted numerical simulations using freely available open-source code Gerris.[30−32] This code uses the volume-of-fluid (VOF) method to solve the incompressible Navier−Stokes equations. The simulations use an axisymmetric geometry and a local adaptive mesh approach, which optimizes the computational cost while resolving the finest structures.

Bubbles bouncing from mobile ethanol or mobile water interfaces were simulated using the generic two-phase VOF Gerris code. In Gerris, the no-slip boundary condition can be defined only for a solid undeformed interface. As in the simulation of a bubble bouncing from an immobile PP1−water interface, our approach to simulating a deformable immobile liquid interface here is to prescribe an effectively higher viscosity of the top phase (e.g., 10 times higher than the bulk liquid viscosity).[27] To be able to do this, we use a three-phase VOF method following the approach recently developed by Chen et al.[33,34] which allows us to use the existing capabilities of the Gerris code to include a top phase with density and viscosity that can be different from that of the rising bubble. In all simulations, the bubble viscosity is identical to that of air, resulting in a tangentially mobile bubble interface. Further details on the Gerris simulation conducted here are given in Supporting Information section S2.

RESULTS AND DICUSSION

Bubble Free-Rise Velocity. First we evaluate the mobility of freely rising bubbles in water and ethanol over the range of bubble sizes investigated. A simple and reliable method to determine the mobility condition on the bubble interface is to measure its terminal free-rise velocity.[16−22] Bubbles with a mobile interface are expected to rise faster. The terminal rise velocity, U_T, in each case depends on the bubble Reynolds number, $Re = \rho DU/\mu$, where ρ is the density of the liquid, μ is the liquid shear viscosity, D is the bubble diameter, and U is the velocity. For very small bubbles of $Re < 0.1$, the mobile bubble rise velocity is expected to be 1.5 times higher than the immobile bubble rise velocity, given by the familiar Stokes' law for solid spheres.[16−18] However, in our experiments bubbles are larger and deform to an oblate ellipsoid shape as shown in Figure 1c. Under such conditions, the clean bubble rise velocity is predicted by Moore's 1965 theory[35] valid for tangentially mobile high-Reynolds-numbers deformable bubbles. Equations giving the bubble rise velocity and shape deformation according to Moore's theory[35] following Manica et al.'s[21] derivation are summarized in the Supporting Information Section S1.

Data for the terminal free-rise velocity of bubbles in water and in ethanol are presented in Figure 2. We cover the size range of 0.6 to 1.5 mm for bubbles in water corresponding to Re = 70 to 460 and 0.6 to 1.2 mm for ethanol corresponding to Re = 50 to 260. In both cases, the bubble free-rise velocity is in excellent agreement with prediction from Moore's theory for the terminal velocity of mobile interface deformable bubbles. For reference, we also show in Figure 2 the immobile spherical bubble terminal rise velocity prediction given by the Schiller−Naumann empirical dependence,[36] which is significantly lower. These measurements confirm that in our experiment the rising bubble water−air and ethanol−air interfaces behaves as tangentially mobile liquid interfaces.

Bubble Bouncing from the Ethanol−Air Interface. First, we discuss measurements for bubbles bouncing from the ethanol−air interface, which we compare with Gerris numerical simulations (GNS) for the case of the mobile and

https://dx.doi.org/10.1021/acs.langmuir.0c00668
Langmuir 2020, 36, 5908−5918

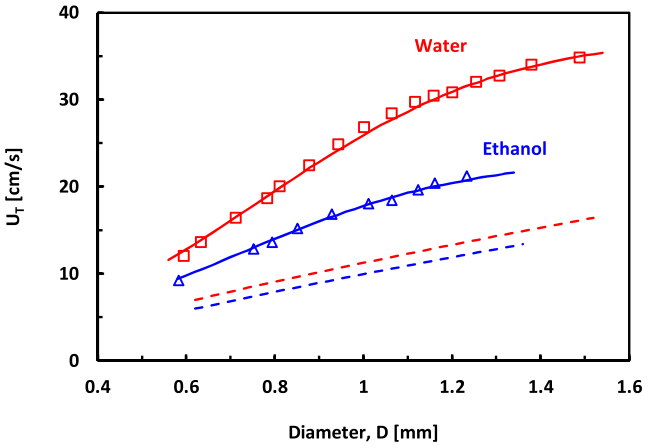

Figure 2. Measured terminal velocities, U_T, of air bubbles freely rising in water (empty squares, red) and in ethanol (empty triangles, blue) vs the undeformed bubble diameter, D. The solid lines are the theoretical predictions using the Moore theory (Supporting Information eqs S1−S6) for mobile deformable bubbles in water (upper solid line, red) and ethanol (lower solid line, blue). The dashed lines show the Schiller−Naumann dependence (Supporting Information eq S7) for immobile interface spherical bubbles in water (upper dashed line, red) and ethanol (lower dashed line, blue).

immobile top liquid interfaces. Video 1 compares the experiment of the bouncing of a D = 1.06 mm bubble from the ethanol−air interface (left) with GNS of the bubble bouncing from mobile (middle) and immobile (right) ethanol−air interfaces. Figure 3a,b shows snapshots from this video for the bubble approaching the interface (Figure 3a) and following the first rebound from the interface (Figure 3b). Figure 3e compares the bubble center-of-mass position vs time dependences extracted from this video. As seen in Video 1 and quantified in Figure 3e, there is good agreement between the experimental and GNS results for the bubble bouncing from the mobile ethanol−air interface. At the same time, the GNS result for the bubble bouncing from the immobile ethanol−air interface gives a significantly weaker bounce (a factor of 1.6 decrease in the maximum rebounding distance). This result is in agreement with our recent experimental and simulation results for the bubble bouncing in perfluorocarbon liquid PP1,[27] which showed a similar increase in bouncing from the mobile PP1−air interface compared to bouncing from an immobile PP1−water interface.

Importantly, we have also found that the bubble rise velocity and the bouncing of the bubble from the interface in ethanol was not affected when different grades of ethanol purity were used or when surfactants were added to the ethanol. An example is given in Video 2 comparing identical sizes of 1.06 mm bubbles bouncing from the interface for pure ethanol (left), ethanol with added 10 mM SDS (middle), and ethanol with added 0.1 wt % AAc (right). Snapshots from this video are shown in Figure 2c,d. Because ethanol is a very good solvent, it is not clear if the SDS or the AAc will preferably adsorb at the ethanol−air interface. However, these experiments demonstrate that the ethanol−air interface mobility is very robust and unlikely to be affected by random contamination. This result is in good agreement with a recent study in which increasing the ethanol concentration in a water−ethanol mixture was used to tune the mixture interface mobility.[37] Thus, perhaps unexpectedly ethanol could be considered to be an alternative model liquid with an inherently

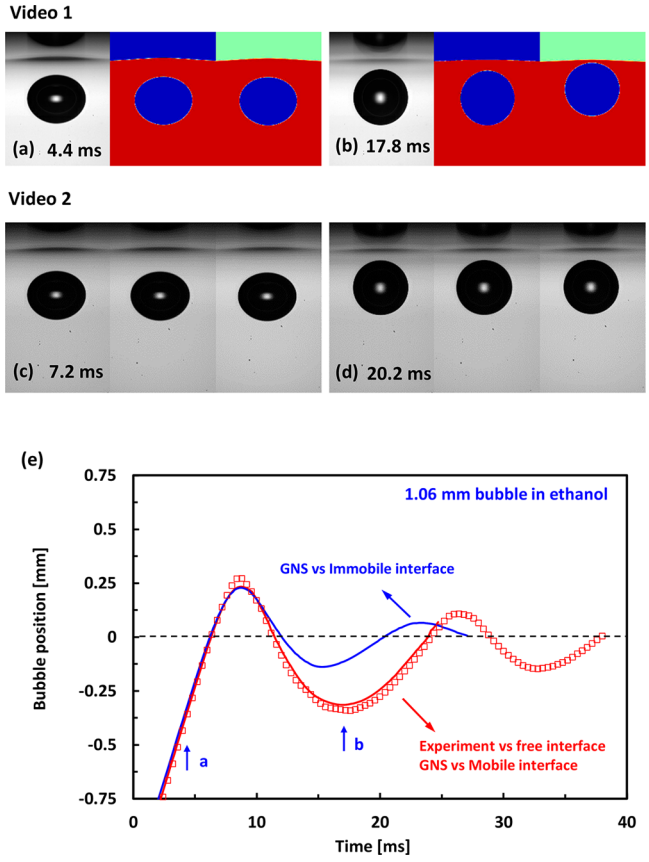

Figure 3. (a, b) Snapshots from Video 1 for D = 1.06 mm bubble bouncing from the ethanol−air interface (left) compared with the GNS of the bubble bouncing from a mobile interface (middle) and an immobile interface (right): bubble approaching the interface (a) and following the first bounce (b). (c, d) Snapshots from Video 2 comparing D = 1.06 mm bubbles bouncing from the interface in pure ethanol (left), ethanol with added 10 mM SDS (middle), and ethanol with added 0.1 wt % AAc (right): bubbles approaching the interface (c) and following the first bounce (d). (e) Bubble center-of-mass position vs time from the experimental data in Video 1 (open red square) compared with GNS results for the bouncing from the mobile interface (lower solid red line) and immobile interface (upper solid blue line).

mobile interface in a manner similar to that for very poor solvent perfluorocarbon liquids. The same might hold for other alcohols and good solvents but should be further examined experimentally.

Bubble Bouncing from the Water−Air Interface. We now compare the bouncing of a free-rising bubble in pure water from the clean water−air interface with the bouncing from a water−air interface on which a Langmuir monolayer of AAc molecules was deposited. As detailed in the Experimental Section, the surface concentration of the AAc monolayer used herein corresponds to a surface area of about 55 Å^2 per molecule and was found to have no measurable effect on the water surface tension value of 72.4 ± 0.1 mN/m.

The comparison of the bubble bounce from the clean water interface with the bubble bounce from the water interface with the AAc monolayer for identical sizes of free-rising bubbles is exemplified in Videos 3, 4, 5, and 6 for the respective cases of D = 0.78, 1.00, 1.30, and 1.50 mm. Snapshots from these videos are presented in Figure 4, and the corresponding bubble

https://dx.doi.org/10.1021/acs.langmuir.0c00668
Langmuir 2020, 36, 5908−5918

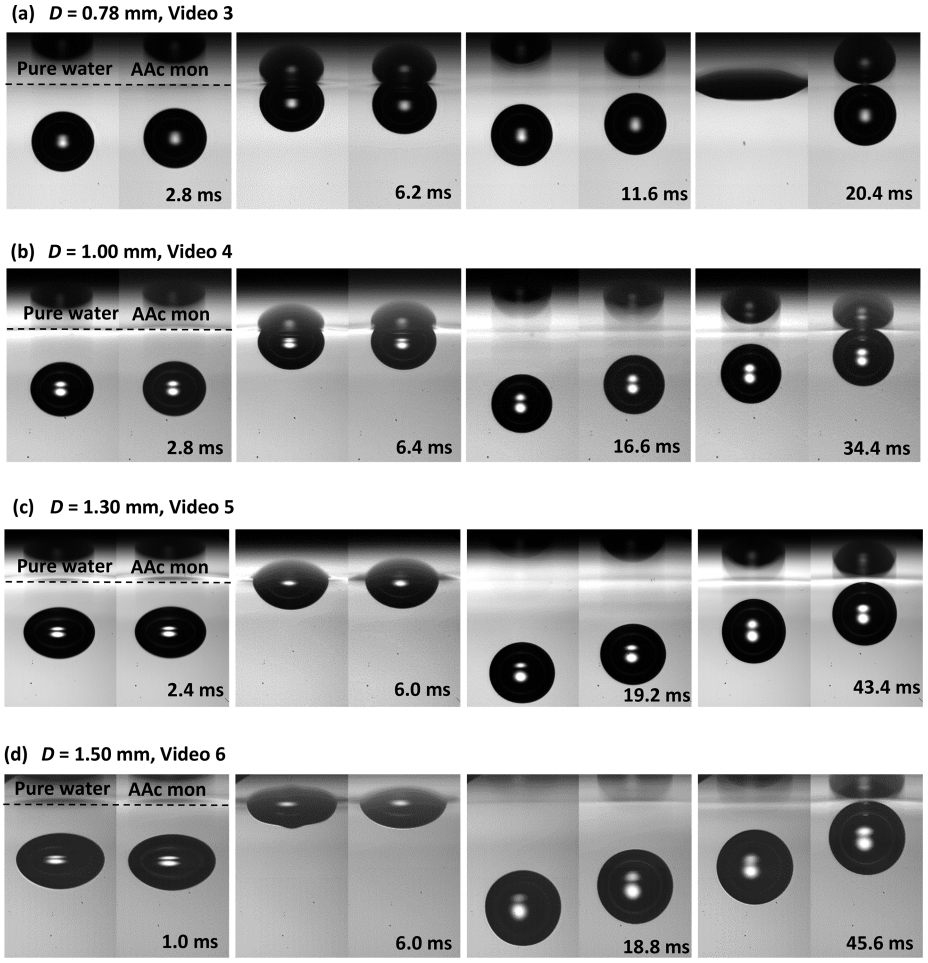

Figure 4. Snapshots showing the bouncing of identical diameter bubbles from the clean water−air interface (left sides) or from the water−air interface with a deposited AAc Langmuir monolayer (right sides): (a) from Video 3 for D = 0.78, (b) from Video 4 for D = 1.00 mm, (c) from Video 5 for D = 1.30, and (d) from Video 6 for D = 1.50 mm. In each set, the first image shows the bubbles approaching the interface, the second image is the first collision with the interface, the third image is after the first bounce, and the fourth is after the second bounce from the interface. Video times in milliseconds are indicated in each snapshot and marked in the Figure 5 center-of-mass position vs time plots.

center-of-mass vs time data, $H(t)$, for each case are presented in Figure 5.

Videos 3 to 6 with Figures 4 and 5 demonstrate that in every case the bubble has a stronger rebound from the clean water−air interface than from the water−air interface with the AAc monolayer. The bounce enhancement effect for the range of bubble sizes studied is further quantified in Figure 6 in terms of the ratio of the maximum amplitudes of the first rebound from the interface, b_m/b_{im} (Figure 5a marking). Bubbles smaller than D = 0.6 mm coalesce with the pure water−air interface without bouncing back. Stronger bouncing varies from about b_m/b_{im} = 1.80 for the D = 0.7 mm bubble to about b_m/b_{im} = 1.20 for the D = 1.5 mm bubble. Even though in terms of the ratio b_m/b_{im} the effect decreases with increasing bubble diameter, it is clearly pronounced for the entire range of bubble sizes studied. Apart from the bounce amplitude, the time duration of each bounce also increases. This larger bounce amplitude and longer duration hold for the consecutive bounces as can be seen in the videos, Figure 4 snapshots, and Figure 5 plots.

In reference measurements, we deposited on the water interface 6 μL of a pure chloroform droplet without added AAc. Following the evaporation of the chloroform, the same bubble bounce was measured as for the pure water interface, confirming that the immobilization of the water interface is due to the AAc Langmuir monolayer. In other experiments, we deposited a slightly higher concentration of the AAc monolayer using 8 μL instead of 6 μL of the 0.1 wt % AAc chloroform solution. No further decrease in the bubble bounce amplitude was noticed, indicating that the standard concentration used in the experiments is high enough to fully immobilize the interface.

We found excellent repeatability between different experimental runs for the H(t) trajectories in experiments both vs pure water and vs the AAc monolayer, as reflected by the small error bars in Figure 6. As could be expected, in this type of experiment,[38−40] there was some variation in the total time before the bubble coalescence with the interface, which was more significant for larger bubbles coalescing with the AAc monolayer deposited interface. Also as can be expected,[14,26,27] the time before coalescence is shorter for the mobile pure water surface than for the immobilized one. However, here we have not conducted a systematic study of the coalescence times, but the trend for faster coalescence at the pure water interface could be noticed in Videos 3, 4, 5, and 6.

These results for bubbles bouncing in water are in agreement with experiments on bubbles bouncing in perfluorocarbon liquid, where stronger bouncing occurs from mobile PP1−air interfaces vs the bounce from an immobile

https://dx.doi.org/10.1021/acs.langmuir.0c00668
Langmuir 2020, 36, 5908−5918

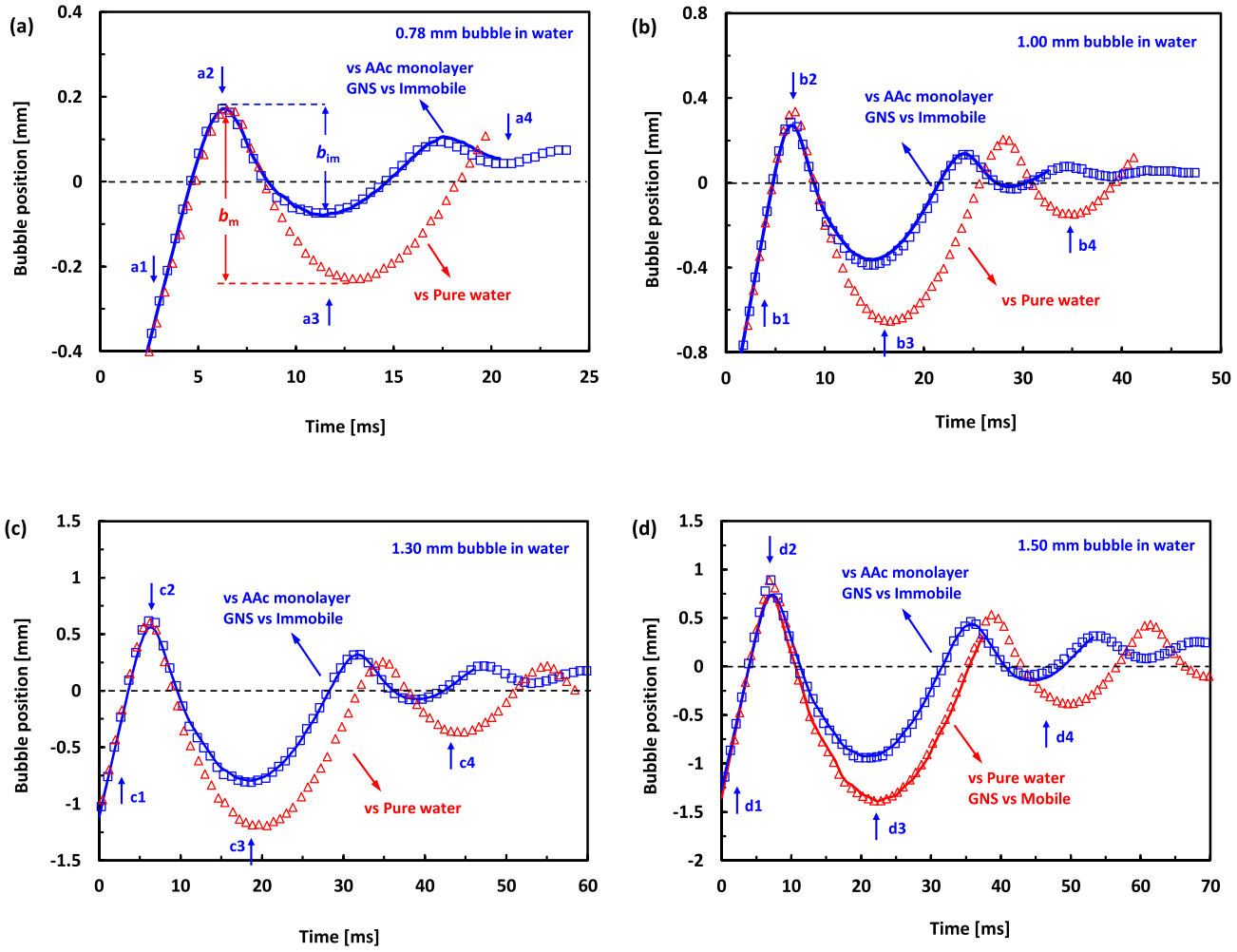

Figure 5. Bubble center-of-mass positions vs time for identical sizes of bubbles bouncing from the pure water−air interface (red triangles) or from the water−air with deposited AAc Langmuir monolayer interface (blue squares) for the cases of (a) D = 0.78 mm (Video 3), (b) D = 1.00 mm (Video 4), (c) D = 1.30 mm (Video 5), and (d) D = 1.50 mm (Video 6). The solid blue lines in each plot represent the GNS results for the bubbles bouncing from the immobile water−air interface (Videos 7, 8, 9, and 10) and the solid red line in (d) for bubble bouncing from the mobile water−air interface (Video 11). The small arrows on each plot mark Figure 4 snapshots positions.

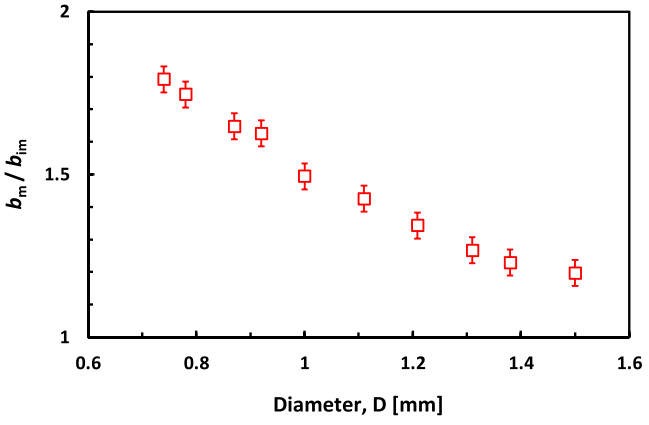

Figure 6. Enhanced bubble bouncing from a pure water surface, compared with the AAc monolayer immobilized water surface, over a range of bubble sizes. The strength of the bouncing is characterized by the ratio of the maximum amplitude of the center-of-mass position after the first rebound, b_m/b_{im}, as marked in Figure 5a.

PP1−water interface with added surfactant.[27] The stronger bounces from the pure water interface indicate that it is a tangentially mobile fluid interface. On the other hand, the water interface with a deposited AAc Langmuir monolayer has the same surface tension but is tangentially immobile.

Gerris Numerical Simulations of a Bubble Bouncing from a Water−Air Interface. We simulate bubbles bouncing from mobile and immobile water−air interfaces using the same approach as for bubbles bouncing from mobile and immobile PP1[27] and ethanol interfaces. For bouncing from a mobile water−air interface, we use two-phase Gerris simulation, and for bubble bouncing from an immobile water−air interface, we use three-phase Gerris simulation,[32] with the top air phase assigned a viscosity that is 10-folds higher than the viscosity of the water to effectively immobilize the fluid interface.

The effectiveness of the high-viscosity-ratio approach to simulating a nearly immobile liquid interface was first demonstrated in our recent study with pure perfluorocarbon liquid, PP1.[27] To examine the use of this approach for the case of the water−air interface, we have simulated the dependence of the terminal rise velocity, U_T, of a D = 0.78 mm bubble on the effective bubble viscosity ratio, $\beta = \mu_{effective}/\mu_{water}$. These results are shown in Supporting Information Figure S2a. As expected for the increase in β, the bubble terminal velocity decreases from the fully mobile value of U_T = 18.8 cm/s at a

https://dx.doi.org/10.1021/acs.langmuir.0c00668
Langmuir 2020, 36, 5908−5918

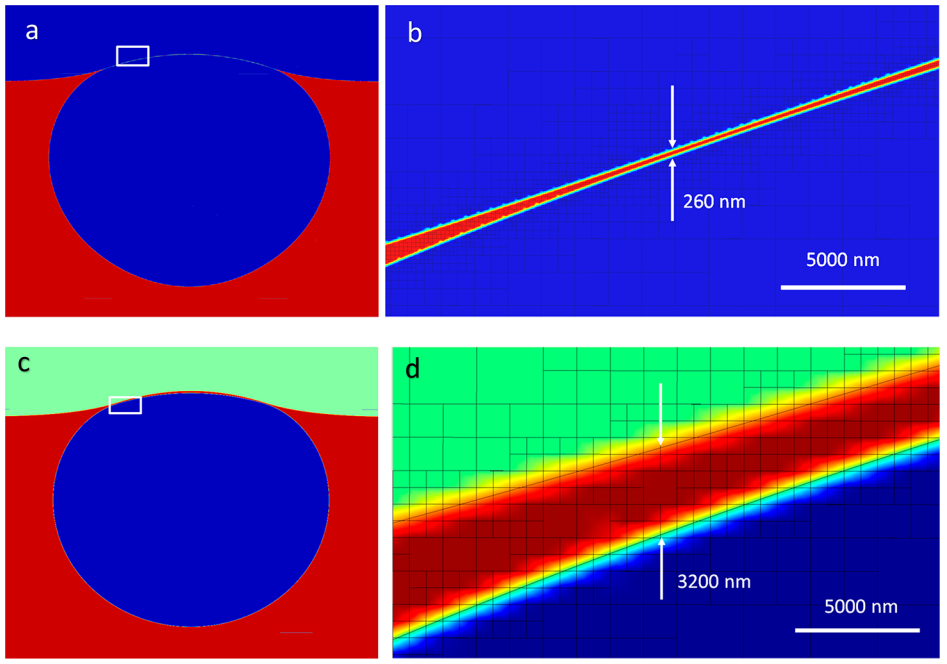

Figure 7. Comparison of the GNS result for the liquid film formed during the bouncing of a 0.78 mm bubble from the mobile and immobile water−air interface. Shown is the moment when the bubbles start to move down. (a) D = 0.78 mm bubble bouncing from the mobile water−air interface and (b) close-up portion indicated by the white area on (a) showing an adaptive mesh of refinement level 17. (c) D = 0.78 mm bubble bouncing from the immobile water−air interface with (d) a close-up portion indicated by the white area on (c) showing an adaptive mesh of refinement level 14.

nominal air viscosity, β = 0.018, to the fully immobile bubble limit of U_T = 8.8 cm/s at higher β, with β = 10 approaching the immobile value within 1% accuracy. Furthermore, using β = 10 for the top air phase, we found excellent agreement with experiments for the bubble bouncing from the immobilized water interface in all cases investigated. In contrast, using β = 1.0 gave an intermediate result between the pure water and immobilized water interface as demonstrated in Supporting Information Figure S2b for the case of a D = 1.00 mm bubble. However, a further increase in β to 20 resulted in a slight decrease in the bubble bounce amplitude, probably due to an effective stiffening of the water−air interface by the higher effective viscosity. Thus, the β = 10 value used in our simulations should be considered to be a semiempirical fitting parameter giving an accurate prediction for the mobile bubble bouncing from an immobile water interface.

Simulations were started with the bubble positioned 22 bubble diameters below the water−air interface, which is a sufficient distance for the bubble to reach terminal rise velocity before colliding with the interface (Supporting Information Figure S1). In the beginning of the simulation, we use adaptive mesh at level 11 refinement. Once the bubble reaches the interface, the simulation refinement level needs to be gradually increased to allow for sufficient resolution to simulate the thin liquid film which forms between the bubble and the interface during the rebound.

For the simulations of the D = 0.78, 1.00, 1.30, and 1.50 mm bubbles bouncing from the immobile water−air interface, the liquid film thins relatively slower and the required maximum refinement level is 15, with a characteristic computational time of few days. However, for the case of bubbles bouncing from a mobile water−air interface the film thins faster and the refinement level needs to be increased much more. The difference in the film thicknesses in the case of mobile and immobile interfaces for the bouncing of a D = 0.78 mm bubble is exemplified in Figure 7, showing a minimum film thickness of about 3200 nm for the immobile interface case vs 260 nm minimum film thickness for the immobile interface, which required level 17 refinement. Even higher refinement levels of up to 18 were required for the D = 1.00 mm bubble and up to 20 for the D = 1.30 mm bubble bouncing from the mobile interface. With the present computational capability, these high refinement levels require very long computational times (months). A related issue is that once the film thickness falls below about 100 nm, surface forces, which are absent from the simulations, such as the electric double layer and van der Waals forces can have a significant impact on the film thinning dynamics. For the cases of bubble bouncing from immobile interfaces, the film thicknesses in our simulations are always much larger than 100 nm during the first and the second bounces from the interface. However, for mobile interfaces during the separation of the bubble from the interface at the end of the first bounce, the film thickness can approach 100 nm. For this reason, here we do not present results for simulations of the bubble bounce from the mobile water−air interfaces in the D = 0.78, 1.00, and 1.30 mm cases.

The only case for which we were able to complete the simulation for the mobile bubble bouncing from the mobile water interface was for the largest D = 1.50 mm bubble. In this case, during the first bounce from the interface the film remains thicker than 230 nm. This allows us to complete the simulation of the first bounce from the mobile interface in reasonable time and also to assume that the effects of surface forces are negligible.

Supporting Information Videos 7, 8, 9, and 10 show side-by-side experiments and GNS for the bubble bounce from the water−air interface on which the AAc monolayer was deposited (i.e., an immobile water−air interface for the

https://dx.doi.org/10.1021/acs.langmuir.0c00668
Langmuir 2020, 36, 5908−5918

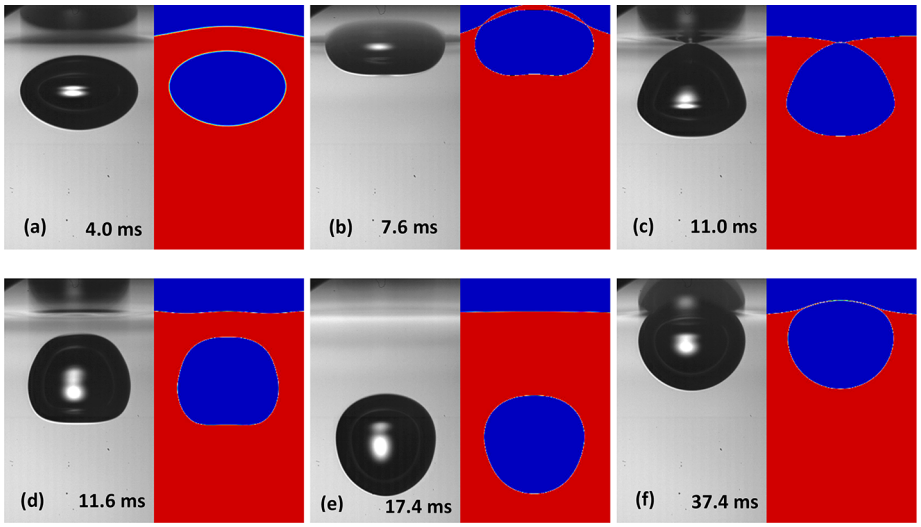

Figure 8. (a–f) Snapshots from Video 11 comparing the bouncing of a 1.50 mm bubble from the pure water–air interface with the GNS simulation of the mobile bubble bouncing from the mobile water–air interface. The time in milliseconds given on each snapshot corresponds to the times in Video 11 and Figure 5d.

respective cases of D = 0.78, 1.00, 1.30, and 1.50 mm bubbles). Solid blue lines in Figure 5 show results from the GNS of the center-of-mass position vs time for bubble bounces from the immobile water–air interface. In all cases, the simulation results are very close to the experimental data for bubbles bouncing from interfaces immobilized by the deposition of the AAc Langmuir monolayer. As can be seen in the videos, the simulations accurately reproduce not only the center of mass vs time position but also the bubble shape oscillation during the larger bubbles rebounding from the interface.

Supporting Information Video 11 shows a side-by-side comparison of the experiment for bouncing from the pure water–air interface with GNS of the same mobile interface for the case of a D = 1.50 mm bubble. The solid red line in Figure 5d shows this simulation result as the center-of-mass position vs time. As in the case of bouncing from the immobile interface, the simulation accurately reproduces not only the center-of-mass position vs time dependence but also the complex way in which the bubble change shape during the bounce. This is highlighted in Figure 8, which shows snapshots from Video 11 comparing the simulation and experimental bubble shape evolution during the bounce. Thus, at least for the largest bubble size of D = 1.50 mm investigated herein, GNS shows that the bouncing from the pure water–air interface is in good agreement with the tangentially mobile boundary condition at the interface and is substantially different from the experimental result for the bubble bouncing from the immobile water–air interface.

Comparison with Prior Studies and Outlook. Our measurements are in very good agreement with prior experimental work for the same systems, for bubbles bouncing from the interface in ethanol with the measurements of Suñol et al.[41] and for bubbles bouncing from the pure water–air interface with the measurements of Zawala et al.[42,43] As we have shown, the ethanol experiments are robust with regards to contamination, and it is not surprising to find good agreement between measurements made in different laboratories (Supporting Information Figure S3a). Measurement in pure water can be more sensitive to the way the experiments are conducted and the water purification protocol. Nevertheless, in converting our bubble position vs time data to velocity vs time data for the bubble bouncing from the pure water interface, we find excellent agreement with the measurements of Zawala et al.[42] for identically sized bubbles (Supporting Information Figure S3b).

Manica et al.[44,45] have proposed an analytical force balance model for the bubble rise, impact, and bounce from a solid surface, which was later adapted for bounces from a fluid interface.[21,46] The model uses the balance of the buoyancy and hydrodynamic drag forces, bubble deformation, inertia of the fluid via an added mass force, and film forces between the bubble and the upper interface. The model demonstrates excellent agreement with the bubble bounce from the pure water interface fitting the experiential data of Zawala et al.[21,42] and the bubble bounce from ethanol interface fitting of the experimental data of Suñol et al.,[21,41] which as we noted above are identical to our measurements. The force balance model used in fitting these data assumes that the top water–air or ethanol–air interface is tangentially immobile.[21] However, according to our study, in both of these cases the bouncing of millimeter-sized bubbles from the clean liquid interface is consistent with the tangentially mobile liquid–air interface, while the bouncing from an immobile interface produces a significantly weaker rebound. We trust that our experimental and simulation results will stimulate the further development of the theoretical models for bubble bouncing from mobile and immobile fluid interfaces to reconcile these disagreements.

Theoretical modeling has the advantage of providing a fast estimate of bubble bouncing from the interface and gives insight into the underlying physical mechanisms.[21,44−46] However, to achieve this the modeling uses a number of approximations, for example, a predetermined bubble shape and an added mass coefficient whose variation near a fluid interface is unknown.[46] The numerical simulations are far more computationally demanding due to the high grid refinement needed to resolve the thin liquid film. On the other hand, the simulation can provide details that are difficult to be obtain by theoretical modeling. One such example, from our prior GNS study, is the emulsion-droplet recoalescence phenomenon caused by inertia effects from the surrounding fluid.[27] Another example, from the present study, is the complex way in which

https://dx.doi.org/10.1021/acs.langmuir.0c00668
Langmuir 2020, 36, 5908−5918

the larger bubble oscillates in shape during the rebound from the interface.

We have now demonstrated that Gerris simulations can accurately model the free rise and bouncing of millimeter-sized mobile-interface bubbles from a mobile liquid interface for different liquids such as perfluorocarbon PP1,[27] ethanol, and water using the experimental spatial and physical parameters of the system and without any fitting parameters. We have also model the bubble bounce from an immobile PP1−water interface and an immobilized water−air interface using a high-viscosity-ratio approach to simulate an immobile liquid interface. Future improvements of the simulation could be a direct application of the immobile boundary condition on fluid interfaces, which is currently unavailable in the Gerris solver. Another major limitation is that surface forces, which become significant for thinner liquid films, are not accounted for in the simulations. One possible approach could be to combine the simulation and the use of lubrication theory[6] once the surfaces are in close contact.

Finally, we want to once more clarify that water−air interface mobility does not depend only on the water purity and the presence of surfactants but is also a strong function of the hydrodynamic regime and related shear rates. Smaller and slow moving bubbles are much easier to immobilize[13−18] compared to larger bubbles subject to higher shear rates.[19−25] Accordingly, all results for the water−air interface mobility discussed here should be considered in the context of the present experiments, which consist of millimeter-sized free-rising bubbles colliding with water−air interfaces.

CONCLUSIONS

Using high-speed camera imaging, we investigated millimeter-sized free-rising bubbles bouncing from mobile and immobile water−air interfaces. This study complements recent results on the effects of the interface mobility on bubbles and droplet collisions in pure perfluorocarbon liquids.[27] It is demonstrated that together with the order of magnitude faster coalescence times,[14,26,27] reflecting the faster drainage rate of the thin liquid film with mobile interfaces, bubbles and droplets with mobile interfaces bounce more strongly due to the lower viscous dissipation during the collision compared to the case of immobile-interface collisions.

We also conducted reference experiments with millimeter-sized bubbles in ethanol, which showed good agreement with the numerical simulation prediction for bubble bounces from the mobile liquid interface. Ethanol was thus found to be an alternative robust mobile-interface liquid. In the case of water, we were able to alter the water−air interface mobility by the deposition of a Langmuir monolayer of AAc. In a series of experiments, 0.7- to 1.5-mm-diameter bubbles freely rising in water were shown to bounce significantly more strongly from the pure water−air interfaces compared to the AAc deposition immobilized water−air interface with the same surface tension. These experiments demonstrate that interface mobility enhances bouncing for the most practically relevant liquid−water. Gerris numerical simulations of bubbles bouncing from mobile and immobile water interfaces correctly reproduce the corresponding experiments of bubbles bouncing from a pure water−air interface and from a water−air interface immobilized by the deposition of a Langmuir monolayer. Importantly, our study provides strong evidence that the clean water−air interface is mobile when millimeter-sized freely rising bubbles are bouncing from it.

ASSOCIATED CONTENT

Supporting Information

The Supporting Information is available free of charge at https://pubs.acs.org/doi/10.1021/acs.langmuir.0c00668.

Moore theory for free-rising bubbles; Gerris direct numerical simulation details; modeling domain; simulated bubble free-rise velocity vs viscosity ratio and simulated bubble bounce from the water-airinterface with various viscosity ratio; comparison with literature data for ethanol and pure water (PDF)

Comparison of the experiment (left) for the D = 1.06 mm bubble bounce from the ethanol−air interface with the GNS result for the bubble bounce from mobile (middle) and immobile (right) ethanol−air interfaces. The time interval per frame is 0.2 ms (5000 fps), and the video is played at 30 fps. (MOV)

Comparison of the bouncing of a D = 1.06 mm bubble from the ethanol−air interface for the case of pure ethanol (left), ethanol with 10 mM SDS (middle), and ethanol with 0.1 wt % AAc (right). The video is recorded at 5000 fps and played at 30 fps. (MOV)

Comparison of the bouncing of a D = 0.78 mm bubble from the pure water−air interface (left) with bouncing from the water−air interface with the AAc monolayer (right). The video is recorded at 5000 fps and played at 30 fps. (MOV)

Comparison of the bouncing of a D = 1.00 mm bubble from the pure water−air interface (left) with bouncing from the water−air interface with the AAc monolayer (right). The video is recorded at 5000 fps and played at 30 fps. (MOV)

Comparison of the bouncing of a D = 1.30 mm bubble from the pure water−air interface (left) with bouncing from the water−air interface with the AAc monolayer (right). The video is recorded at 5000 fps and played at 30 fps. (MOV)

Comparison of the bouncing of a D = 1.50 mm bubble from the pure water−air interface (left) with bouncing from the water−air interface with the AAc monolayer (right). The video is recorded at 5000 fps and played at 30 fps. (MOV)

Comparison of the experiment (left) for the D = 0.78 mm bubble bounce from the water−air interface with the AAc monolayer with the GNS result (right) for the bubble bounce from the immobile water−air interface. The time interval per frame is 0.2 ms (5000 fps), and the video is played at 30 fps. (MOV)

Comparison of the experiment (left) for the D = 1.00 mm bubble bounce from the water−air interface with the AAc monolayer with the GNS result (right) for the bubble bounce from the immobile water−air interface. The time interval per frame is 0.2 ms (5000 fps), and the video is played at 30 fps. (MOV)

Comparison of the experiment (left) for the D = 1.30 mm bubble bounce from the water−air interface with the AAc monolayer with the GNS result (right) for the bubble bounce from the immobile water−air interface. The time interval per frame is 0.2 ms (5000 fps), and the video is played at 30 fps. (MOV)

Comparison of the experiment (left) for the D = 1.50 mm bubble bounce from the water−air interface with the AAc monolayer with the GNS result (right) for the

https://dx.doi.org/10.1021/acs.langmuir.0c00668
Langmuir 2020, 36, 5908−5918

bubble bounce from the immobile water−air interface. The time interval per frame is 0.2 ms (5000 fps), and the video is played at 30 fps. (MOV)

Comparison of the experiment (left) for the D = 1.50 mm bubble bounce from the pure water−air interface with the GNS result (right) for the bubble bounce from the mobile water−air interface. The time interval per frame is 0.2 ms (5000 fps), and the video is played at 30 fps. (MOV)

AUTHOR INFORMATION

Corresponding Author

Ivan U. Vakarelski − *Division of Physical Sciences and Engineering, King Abdullah University of Science and Technology (KAUST), Thuwal 23955-6900, Saudi Arabia;* orcid.org/0000-0001-9244-9160; Email: ivanuriev.vakarelski@kaust.edu.sa

Authors

Fan Yang − *Division of Physical Sciences and Engineering, King Abdullah University of Science and Technology (KAUST), Thuwal 23955-6900, Saudi Arabia*

Sigurdur T. Thoroddsen − *Division of Physical Sciences and Engineering, King Abdullah University of Science and Technology (KAUST), Thuwal 23955-6900, Saudi Arabia;* orcid.org/0000-0001-6997-4311

Complete contact information is available at: https://pubs.acs.org/10.1021/acs.langmuir.0c00668

Notes

The authors declare no competing financial interest.

ACKNOWLEDGMENTS

We acknowledge the use of the Gerris solver in our investigation. The experimental and computational work was supported by the King Abdullah University of Science and Technology (KAUST) under grant URF/1/3723-01-01.

REFERENCES

(1) Chesters, A. K. Modelling of coalescence processes in fluid-liquid dispersions: a review of current understanding. *Chem. Eng. Res. Des.* **1991**, *69*, 259−270.

(2) Ivanov, I. D.; Kralchevsky, P. A. Stability of emulsions under equilibrium and dynamic conditions. *Colloids Surf., A* **1997**, *128*, 155−175.

(3) Sanfeld, A.; Steinchen, A. Emulsions stability, from dilute to dense emulsions — Role of drops deformation. *Adv. Colloid Interface Sci.* **2008**, *140*, 1−65.

(4) Liao, Y.; Lucas, D. A literature review on mechanisms and models for the coalescence process of fluid particles. *Chem. Eng. Sci.* **2010**, *65*, 2851−2864.

(5) Vakarelski, I. U.; Manica, R.; Tang, X. S.; O'Shea, S. J.; Stevens, G. W.; Grieser, F.; Dagastine, R. R.; Chan, D. Y. C. Dynamic interactions between microbubbles in water. *Proc. Natl. Acad. Sci. U. S. A.* **2010**, *107*, 11177−11182.

(6) Chan, D. Y. C.; Manica, R.; Klaseboer, E. Film drainage and coalescence between deformable drops and bubbles. *Soft Matter* **2011**, *7*, 2235−2264.

(7) Kamp, J.; Villwock, J.; Kraume, M. Drop coalescence in technical liquid/liquid applications: A review on experimental techniques and modelling approaches. *Rev. Chem. Eng.* **2017**, *33*, 1−47.

(8) Xie, L.; Shi, C.; Cui, X.; Zeng, H. Surface forces and interaction mechanisms of emulsion drops and gas bubbles in complex fluids. *Langmuir* **2017**, *33*, 3911−3925.

(9) Chesters, A. K.; Hofman, G. Bubble coalescence in pure liquids. *Appl. Sci. Res.* **1982**, *38*, 353−361.

(10) Abid, S.; Chesters, A. K. The drainage and rupture of partially-mobile films between colliding drops at constant approach velocity. *Int. J. Multiphase Flow* **1994**, *20*, 613−628.

(11) Yoon, Y.; Baldessari, F.; Ceniceros, H. D.; Leal, L. G. Coalescence of two equal-sized deformable drops in an axisymmetric flow. *Phys. Fluids* **2007**, *19*, 102102.

(12) Manor, O.; Vakarelski, I. U.; Stevens, G. W.; Grieser, F.; Dagastine, R. R.; Chan, D. Y. C. Dynamic forces between bubbles and surfaces and hydrodynamic boundary conditions. *Langmuir* **2008**, *24*, 11533−11543.

(13) Manica, R.; Hendrix, M. H. W.; Gupta, R.; Klaseboer, E.; Ohl, C.-D.; Chan, D. Y. C. Effects of hydrodynamic film boundary conditions on bubble-wall impact. *Soft Matter* **2013**, *9*, 9755−9758.

(14) Liu, B.; Manica, R.; Liu, Q.; Klaseboer, E.; Xu, Z.; Xie, G. Coalescence of bubbles with mobile interfaces in water. *Phys. Rev. Lett.* **2019**, *122*, 194501.

(15) Carnie, S. C.; Del Castillo, L.; Horn, R. G. Mobile surface charge can immobilize the air/water interface. *Langmuir* **2019**, *35* (5), 16043−16052.

(16) Parkinson, L.; Sedev, R.; Fornasiero, D.; Ralston, J. The terminal rise velocity of 10−100 μm diameter bubbles in water. *J. Colloid Interface Sci.* **2008**, *322*, 168−172.

(17) Kelsall, G. H.; Tang, S.; Smith, A. L.; Yurdakul, S. Measurement of rise and electrophoretic velocities of gas bubbles. *J. Chem. Soc., Faraday Trans.* **1996**, *92*, 3879−3885.

(18) Pawliszak, P.; Ulaganathan, V.; Bradshaw-Hajek, B. H.; Manica, R.; Beattie, D. A.; Krasowska, M. Mobile or immobile? Rise velocity of air bubbles in high-purity water. *J. Phys. Chem. C* **2019**, *123*, 15131−15138.

(19) Malysa, K.; Krasowska, M.; Krzan, M. Influence of surface active substances on bubble motion and collision with various interfaces. *Adv. Colloid Interface Sci.* **2005**, *114*−*115*, 205−225.

(20) Fujasová-Zedníková, M.; Vobecká, L.; Vejrazka, J. Effect of solid material and surfactant presence on interactions of bubbles with horizontal solid surface. *Can. J. Chem. Eng.* **2010**, *88*, 473−481.

(21) Manica, R.; Klaseboer, E.; Chan, D. Y. C. The impact and bounce of air bubbles at a flat fluid interface. *Soft Matter* **2016**, *12*, 3271−3282.

(22) Zawala, J.; Malysa, K.; Kowalczuk, P. B. On importance of external conditions and properties of the interacting phases in formation and stability of symmetrical and unsymmetrical liquid films. *Adv. Colloid Interface Sci.* **2020**, *276*, 102085.

(23) Denkov, N. D.; Tcholakova, S.; Golemanov, K.; Ananthpadmanabhan, K. P.; Lips, A. The role of surfactant type and bubble surface mobility in foam rheology. *Soft Matter* **2009**, *5*, 3389−3408.

(24) Vakarelski, I. U.; Klaseboer, E.; Jetly, A.; Mansoor, M. M.; Aguirre-Pablo, A. A.; Chan, D. Y. C.; Thoroddsen, S. T. Self-determined shapes and velocities of giant near-zero drag gas cavities. *Sci. Adv.* **2017**, *3*, No. e1701558.

(25) Vakarelski, I. U.; Jetly, A.; Thoroddsen, S. T. Stable-streamlined cavities following the impact of non-superhydrophobic spheres on water. *Soft Matter* **2019**, *15*, 6278−6287.

(26) Vakarelski, I. U.; Manica, R.; Li, E. Q. E. S.; Basheva, E. S.; Chan, D. Y. C.; Thoroddsen, S. T. Coalescence dynamics of mobile and immobile fluid interfaces. *Langmuir* **2018**, *34*, 2096−2108.

(27) Vakarelski, I. U.; Yang, F.; Tian, Y. S.; Li, E. Q.; Chan, D. Y. C.; Thoroddsen, S. T. Mobile-surface bubbles and droplets coalesce faster but bounce stronger. *Sci. Adv.* **2019**, *5*, No. eaaw4292.

(28) Langmuir, I. The constitution and fundamental properties of solids and liquids: II. Liquids. *J. Am. Chem. Soc.* **1917**, *39*, 1848−1906.

(29) Kaganer, V. M.; Möhwald, H.; Dutta, P. Structure and phase transitions in Langmuir monolayers. *Rev. Mod. Phys.* **1999**, *71*, 778−891.

(30) Popinet, S. *Gerris Flow Solver*, http://gfs.sf.net.

(31) Popinet, S. An accurate adaptive solver for surface-tension-driven interfacial flows. *J. Comput. Phys.* **2009**, *228*, 5838−5866.

https://dx.doi.org/10.1021/acs.langmuir.0c00668
Langmuir 2020, 36, 5908−5918

(32) Fuster, D.; Agbaglah, G.; Josserand, C.; Popinet, S.; Zaleski, S. Numerical simulation of droplets, bubbles and waves: state of the art. *Fluid Dyn. Res.* **2009**, *41*, 065001.
(33) Chen, X.; Sun, Y.; Xue, C.; Yu, Y.; Hu, G. Tunable structures of compound droplets formed by collision of immiscible microdroplets. *Microfluid. Nanofluid.* **2017**, *21*, 109.
(34) Wang, B.; Wang, C.; Yu, Y.; Chen, X. Spreading and penetration of a micro-sized water droplet impacting onto oil layers. *Phys. Fluids* **2020**, *32*, 012003.
(35) Moore, D. W. The velocity of rise of distorted gas bubbles in a liquid of small viscosity. *J. Fluid Mech.* **1965**, *23*, 749−766.
(36) Schiller, L.; Naumann, A. A drag coefficient correlation. *Z. Ver. Deutsch. Ing.* **1935**, *77*, 318−320.
(37) Zhang, X.; Manica, R.; Tang, Y.; Liu, Q.; Xu, Z. Bubbles with tunable mobility of surfaces in ethanol-NaCl aqueous solutions. *J. Colloid Interface Sci.* **2019**, *556*, 345−351.
(38) Li, E. Q.; Vakarelski, I. U.; Chan, D. Y. C.; Thoroddsen, S. T. Stabilization of thin liquid films by repulsive van der Waals force. *Langmuir* **2014**, *30*, 5162−5169.
(39) Katsir, Y.; Marmur, A. Rate of bubble coalescence following dynamic approach: collectivity-induced specificity of ionic effect. *Langmuir* **2014**, *30*, 13823−13830.
(40) Langevin, D. Bubble coalescence in pure liquids and in surfactant solutions. *Curr. Opin. Colloid Interface Sci.* **2015**, *20*, 92−97.
(41) Suñol, F.; González-Cinca, R. Rise, bouncing and coalescence of bubbles impacting at a free surface. *Colloids Surf., A* **2010**, *365*, 36−42.
(42) Zawala, J.; Malysa, K. Influence of the impact velocity and size of the film formed on bubble coalescence time at water surface. *Langmuir* **2011**, *27*, 2250−2257.
(43) Zawala, J.; Dorbolo, S.; Vandewalle, N.; Malysa, K. Bubble bouncing at a clean water surface. *Phys. Chem. Chem. Phys.* **2013**, *15*, 17324−17332.
(44) Manica, R.; Klaseboer, E.; Chan, D. Y. C. Force balance model for bubble rise, impact, and bounce from solid surfaces. *Langmuir* **2015**, *31*, 6763−6772.
(45) Manica, R.; Klaseboer, E.; Chan, D. Y. C. The hydrodynamics of bubble rise and impact with solid surfaces. *Adv. Colloid Interface Sci.* **2016**, *235*, 214−232.
(46) Emery, T. S.; Kandlikar, S. G. Modeling bubble collisions at liquid-liquid and compound interfaces. *Langmuir* **2019**, *35*, 8294−8307.

https://dx.doi.org/10.1021/acs.langmuir.0c00668
Langmuir 2020, 36, 5908−5918